Original Research

Semiautomated Method for Noise Reduction and Background Phase Error Correction in MR Phase Velocity Data[1]

Peter G. Walker, PhD • Gregory B. Cranney, MD • Markus B. Scheidegger, PhD
Gena Waseleski, BChE • Gerald M. Pohost, MD • Ajit P. Yoganathan, PhD

Background phase distortion and random noise can adversely affect the quality of magnetic resonance (MR) phase velocity measurements. A semiautomated method has been developed that substantially reduces both effects. To remove the background phase distortion, the following steps were taken: The time standard deviations of the phase velocity images over a cardiac cycle were calculated. Static regions were identified as those in which the standard deviation was low. A flat surface representing an approximation to the background distortion was fitted to the static regions and subtracted from the phase velocity images to give corrected phase images. Random noise was removed by setting to zero those regions in which the standard deviation was high. The technique is demonstrated with a sample set of data in which the in-plane velocities have been measured in an imaging section showing the left ventricular outflow tract of a human left ventricle. The results are presented in vector and contour form, superimposed on the conventional MR angiographic images.

Index terms: Heart, flow dynamics, 51.12144 • Heart, function, 51.12144 • Heart, MR, 51.12144 • Heart, ventricles, 524.12144 • Image display • Image processing • Phase correction • Phase imaging • Vascular studies • Velocity studies

JMRI 1993; 3:521–530

Abbreviation: LVOT = left ventricular outflow tract.

THE FLOW OF BLOOD through the cardiovascular system is a critical factor in the pathogenesis of a number of disorders. For instance, the flow in the carotid artery and other bifurcations has long been suspected of influencing the location and severity of sclerotic plaque (1–4), and the flow in the left ventricle is thought to be a factor in the mechanics of the mitral valve (5) and in thrombus formation (6). To understand and investigate this interaction between blood flow and its surroundings, it is vital that a clear qualitative assessment and an accurate quantitative measurement of the flow velocity field be obtained. One method that allows us to do this in the human body is magnetic resonance (MR) phase velocity encoding (7–10). With this technique, the velocity field can be measured over an MR imaging section.

Problems with this method can arise, however, when measurement errors due to regions of noisy data and background phase distortions impair the quality of the phase velocity data. Noisy regions can result when air is present (eg, in the lungs). On a typical angiographic image representation of velocity, noise is not a great problem. For other representations, such as vector plots, abnormally large velocity vectors from the noisy regions can overlap important areas and impair interpretation of plots. Background phase distortion arises from inhomogeneities in the magnetic field and eddy current effects and will result in an incorrect velocity measurement.

Herein a method is presented for the removal of noise and background distortion from MR phase velocity images. Because there can be a large number of such images in a single study, it is not feasible to perform time-consuming interactive processing, as others have done (11). The method presented here is, therefore, semiautomated, requiring only two input parameters from the operator before processing and requiring no regions of interest. An acquisition time of 15 minutes and a postprocessing time of 5 minutes makes the method feasible for on-site, immediate use.

To demonstrate the method, results of a study are presented in which the two in-plane velocity components have been measured in the left ventricular

[1] From the School of Chemical Engineering, Georgia Institute of Technology, 888 Hemphill Ave, Atlanta, GA 30332-0100 (P.G.W., G.W., A.P.Y.); and Department of Cardiovascular Disease, School of Medicine, University of Alabama at Birmingham, Birmingham, (G.B.C., M.B.S., G.M.P.). Received July 22, 1992; revision requested September 15; revision received and accepted November 16. **Address reprint requests to** P.G.W.

outflow tract (LVOT) of a healthy human heart. The results are presented in a form that provides a qualitative and quantitative understanding of the flow field and insight into the interaction between flow and surrounding tissue.

• METHODS

MR Measurements

The imaging plane was an LVOT view, in which the mitral and aortic valves and the left ventricle and atrium were visible (Fig 2a). The pulmonary artery, descending aorta, right atrium, and superior vena cava are also seen in the image. Twenty images spaced 39 msec apart were obtained per heart cycle, with the first image acquired 14 msec after the electrocardiograph R wave. A 1.5-T S-15 MR system (Philips Medical Systems, Shelton, Conn), based at the University of Alabama at Birmingham, was used, with the FLAG (flow-adjusted gradient) flow quantification procedure. With this method, the velocity-sensitive pulse sequence is interleaved with the velocity-compensated sequence at each encoding step. A more detailed description of the sequence is given in reference 12. The following parameters were used: 128 × 128 resolution, 400-mm field of view, two signals averaged, 10-msec TE, 8-mm section thickness, and 45° flip angle. The two in-plane velocity components were measured, with the velocity range set at −166 to 165 cm/sec. The initial phase subtraction was performed with the MR Vax computer (Digital Equipment, Maynard, Mass) immediately after imaging. The portions of the data corresponding to the heart were extracted from the full image by using the trackball on the MR console. For the data set presented here, the extracted portion was 25 × 35 pixels. The resulting modulus and velocity files were then transferred to a Personal Iris 4D25G workstation (Silicon Graphics, Mountain View, Calif) at the Georgia Institute of Technology, where the following data analysis was performed.

Data Analysis

Background phase error correction.—The procedure to remove the background phase errors relies on the time standard deviation of the velocity and is performed for the horizontal velocity images, V, and the vertical velocity images, U, separately. The analysis is the same for both velocity components, but for brevity only the horizontal component is presented, as follows:

1. Calculate a time mean, $V_{mean}(x,y)$, of the phase velocity–encoded images over a heart cycle (Fig 1b). This can be expressed mathematically as

$$V_{mean}(x,y) = \frac{1}{N}\sum_{n=1}^{N} V(x,y,n), \quad (1)$$

where $V(x,y,n)$ is the velocity at voxel position (x,y) in the nth image in the heart cycle and N is the total number of images ($N = 20$ for this data set).

2. Calculate the time standard deviation of the images about this mean (Fig 1c) with the following equation:

$$V_{sd}(x,y) = \sqrt{\frac{1}{N}\sum_{n=1}^{N} [V_{mean}(x,y) - V(x,y,n)]^2}, \quad (2)$$

where $V_{sd}(x,y)$ is the time standard deviation of the velocity data at voxel location (x,y).

3. Locate the static regions of each velocity image throughout the cardiac cycle, $V_{static}(x,y,n)$. These are defined as the regions in which the standard deviation is below a certain limit. The standard deviation image represents the degree of velocity fluctuation in each voxel. Static regions of the image will therefore have a small standard deviation because the velocity at these locations will not vary appreciably throughout the cardiac cycle. Other regions, such as those corresponding to the air surrounding the patient, are noisy and have a high standard deviation. Regions corresponding to flowing blood have a pulsatile nature and a medium standard deviation. Both regions can therefore be separated from the static regions on the basis of the magnitude of the standard deviation.

The cutoff limit (*limit* in Eq [3]) for the static regions was chosen to be that value of the standard deviation below which 15% of the standard deviation data lay (Fig 1d), or

$$V_{static}(x,y,n) = V(x,y,n), \quad \text{if} \quad V_{sd}(x,y) < \text{limit}. \quad (3)$$

4. For each image in the heart cycle, a plane surface is fitted to the velocity data in the static regions of the image (Fig 1e). It is not possible to exactly fit a flat surface to the static velocity regions because the variation across the images is not purely linear. An approximation to the data must therefore be sought that creates a best fit. For this analysis, a least-squares fit is used. The plane has an equation of the form:

$$V_{error}(x,y,n) = Ax + By + D, \quad (4)$$

where $V_{error}(x,y,n)$ is the height of the plane at location (x,y) and represents an approximation to the background phase (or velocity) error for the nth image in the heart cycle. A, B, and D are constants that define the orientation of the plane and are determined from the following equations:

$$B = \frac{[(C_{zx} \times C_{xy}) - (C_{zy} \times C_{xx})]}{[(C_{xy} \times C_{xy}) - (C_{yy} \times C_{xx})]}, \quad (5)$$

$$A = \frac{[C_{zx} - (B \times C_{xy})]}{C_{xx}}, \quad (6)$$

$$D = Z - AX - BY, \quad (7)$$

where $C_{ij} = P(n) \times I \times J - (I \times J)$ and $I = \Sigma i$; $J = \Sigma j$; $X = \Sigma x$; $Y = \Sigma y$; $Z = \Sigma V_{static}(x,y,n)$. These summations are taken over the data in the static regions only, as defined above. $P(n)$ is the total number of data points in the static regions of the nth image in a cardiac cycle.

5. For each image in the heart cycle, the corresponding error plane is subtracted from the velocity image to give a background error–corrected velocity image (Fig 1f), or

$$V_{bge}(x,y,n) = V(x,y,n) - V_{error}(x,y,n), \quad (8)$$

where $V_{bge}(x,y,n)$ are the background error–corrected velocity images.

Random noise error correction.—The following procedure defines random noise and sets the velocity

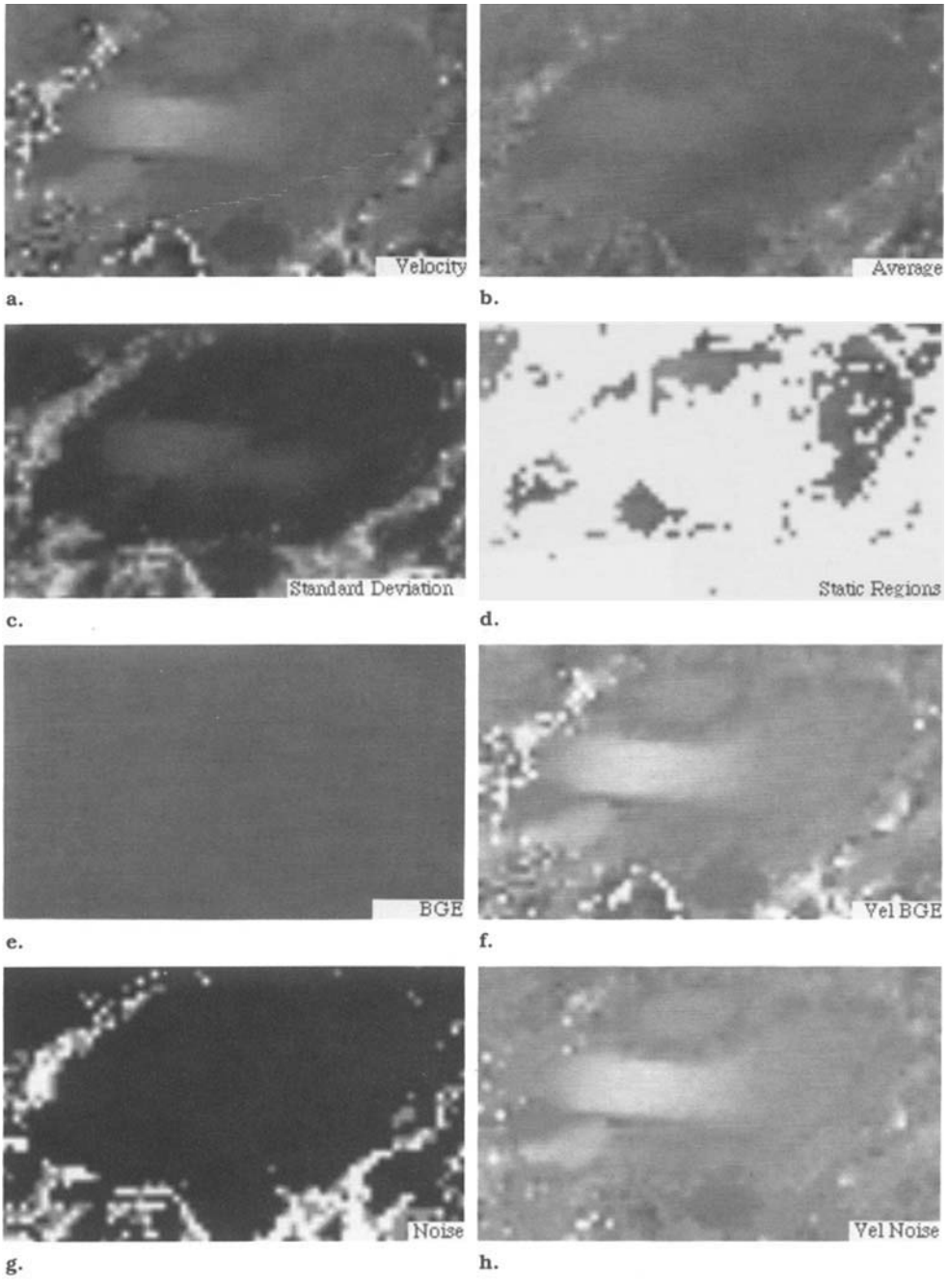

Figure 1. Steps in the removal of the background phase error and noise include **(a)** the initial phase image, **(b)** the time average phase image, **(c)** the time standard deviation image, **(d)** the low-standard-deviation (static regions) image, **(e)** the background error image, **(f)** the velocity image with the background error subtracted, **(g)** the image showing the regions of noise (all pixels that are not black correspond to noise), and **(h)** the final velocity image with the background error and noise removed.

in these voxels equal to zero:

1. Steps 1 and 2 of the background phase error correction procedure are repeated for both the horizontal and vertical velocity components. The result is a standard deviation image for each velocity component measured.

2. The noisy areas for each velocity component are found. For each velocity component, a mask image is created that consists of 0's and 1's, so that a 1 appears in areas in which the standard deviation exceeds a predetermined limit; all other areas are set to 0. In doing this, it is assumed that noisy regions have a large standard deviation. This can be expressed mathematically as $V_{mask}(x,y) = 1$, if $V_{sd}(x,y) >$ limit; $U_{mask}(x,y) = 1$, if $U_{sd}(x,y) >$ limit; or $V_{mask}(x,y) = 0$, if $V_{sd}(x,y) <$ limit; $U_{mask}(x,y) = 0$, if $U_{sd}(x,y) <$ limit, where $V_{mask}(x,y)$ and $U_{mask}(x,y)$ are mask images for the horizontal and vertical velocity components, respectively.

3. The mask images are summed to form a noise image (Fig 1g),

$$\text{Noise}(x,y) = V_{mask}(x,y) + U_{mask}(x,y). \quad (9)$$

4. In all the velocity images, the velocity is set to zero at those locations in which the noise image exceeds 1. In other words, the standard deviation must

be large for both velocity components for the velocity in that voxel to be defined as being due to random noise (Fig 1h), or

$$V_{noise}(x,y,n) = 0, \quad \text{if} \quad Noise(x,y) = 2,$$
$$U_{noise}(x,y,n) = 0, \quad \text{if} \quad Noise(x,y) = 2;$$

or (10)

$$V_{noise}(x,y,n) = V_{bge}(x,y,n),$$
$$U_{noise}(x,y,n) = U_{bge}(x,y,n).$$

$V_{noise}(x,y,n)$ and $U_{noise}(x,y,n)$ represent the final background error–corrected and noise-reduced horizontal and vertical velocity images, respectively.

Visualization of the final velocity field.—After the two error reduction procedures have been performed, the final velocity images are displayed in vector and contour form. The contours show the magnitude of the in-plane velocity vector, $V_{mag}(x,y,n)$, as calculated by

$$V_{mag}(x,y,n) = \sqrt{[V_{noise}(x,y,n)^2 + U_{noise}(x,y,n)^2]}. \quad (11)$$

Both the contour and vector plots are superimposed on the modulus image in order to place the data in relation to the morphology of the heart. In this way, the interaction between the flowing blood and moving walls and valves of the heart can be studied. As with the images generated on the Philips machine console, the figures shown here have been linearly interpolated to enhance image quality. No smoothing of the data is performed. The contour overlays have not been interpolated, and the vector overlays have been desampled to reduce crowding.

• RESULTS

Figures 1 and 2 show the LVOT view of the left ventricle, with the anatomy labeled in Figure 2a. The left ventricle is located in the right half of the image, with the LVOT and aorta just left of center and the apex at the top right. The right atrium is at the top center and the left atrium just below the center. The descending aorta is at the bottom.

Data Analysis

The various steps in the data analysis are demonstrated in Figure 1, with the data for the horizontal velocity component. The data are shown as gray scale raster images, with black corresponding to a low or negative velocity and white to a high and positive velocity. Figure 1a, 1b, 1e, 1f, and 1h have the same scaling to make them comparable. On these images, black corresponds to a velocity of −166 cm/sec and white to 165 cm/sec. For the other images (Fig 1c, 1d, 1g) the scaling has been chosen to fit the range of the data.

Figure 1a shows the unprocessed initial velocity image $V(x,y,n)$, obtained after phase subtraction for an image in midsystole ($n = 3$). The flow from the ventricle is near its maximum and is shown as the white band across the center of the image. Regions of noise surround a substantial portion of the heart and are seen as speckled areas. The background phase error is evident in the dark appearance of the image; if no error were present, the image would have a middle gray tone, which represents zero velocity.

Figure 1b shows the time mean image for the horizontal velocity data. Because of the pulsatile nature of the flow, the mean velocity tends to be near zero everywhere, giving the image a flat appearance.

Figure 1c shows the time standard deviation image. This image reflects the magnitude of the velocity fluctuations in each voxel. The noisy areas have a high standard deviation and appear brightest. These areas surround the heart and do not degrade the appearance of the important regions of flow. Since the standard deviation is always positive, black corresponds to zero on this image. Static regions that have a low standard deviation therefore appear dark. Pulsatile flow regions, such as in the LVOT and mitral inflow regions, have a standard deviation between the high standard deviation of the noisy regions and the low deviation of the static regions and are represented by gray.

Figure 1d shows the static regions of the image. These regions coincide with the darkest regions of Figure 1c, where the standard deviation is low. On the image, the gray scale has been adjusted to range from −166 cm/sec to zero. This range is smaller than that in Figure 1a, and therefore the velocity gradients within the image are enhanced. Since all the static regions should have approximately the same velocity, any variation over these regions is due to the background phase error. In Figure 1d, it is evident that the static regions in the top left corner have a less negative value than those on the right side of the image. Any correction to the background error must therefore take this gradient into account.

The background phase error correction is shown in Figure 1e. This image shows the plane that was fitted to the static region data shown in Figure 1d. In this particular case, the background error shows a large offset but a relatively small gradient. In other studies that we have performed, the slope of the background error has been relatively large.

Figure 1f shows the velocity image (Fig 1a) with the background phase image (Fig 1e) subtracted.

Figure 1g shows the noisy areas of the image. The image is composed of 0's, 1's, and 2's, with 0's as black, 1's as gray, and 2's as white. A 0 appears wherever the standard deviations of both the horizontal and vertical velocity images are below a preset limit (see below). Likewise, 1's appear wherever one of the two standard deviations is above the limit, and 2's appear wherever both standard deviations are above the limit. This image, therefore, represents a correlation between the regions of high standard deviation in the horizontal and vertical velocity images. Areas in which the 2's appear are defined as noisy areas and are set to zero magnitude in the velocity images.

Figure 1h is the final velocity image, with both background error and noise removed. Comparing it with Figure 1f, in which the noise is still present, it can be seen that the noise has been substantially—although not totally—removed.

Visualization

Figure 2 shows the final vector and contour plots. Every other image obtained over the cardiac cycle is shown. The vector plots are on the left and the contour plots on the right. Although the size of the vector

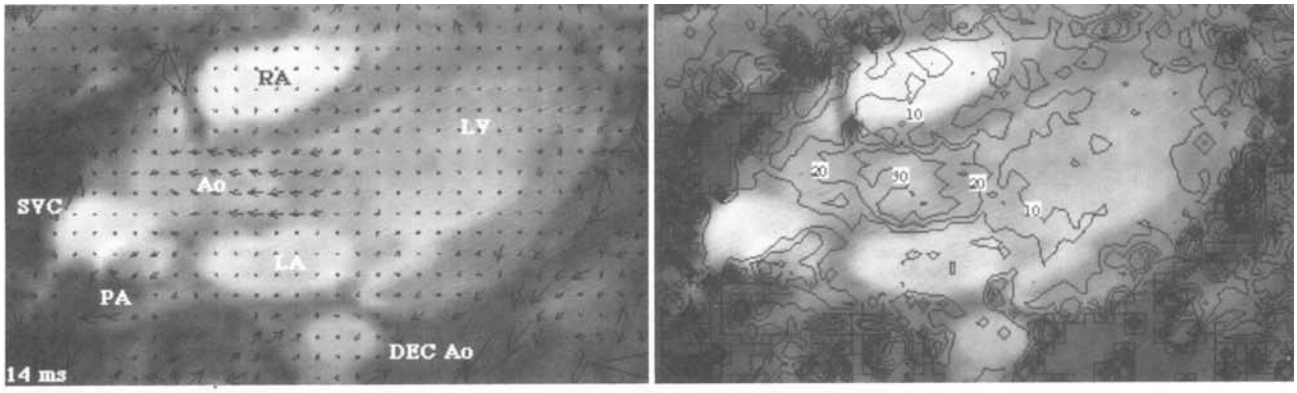

2a.

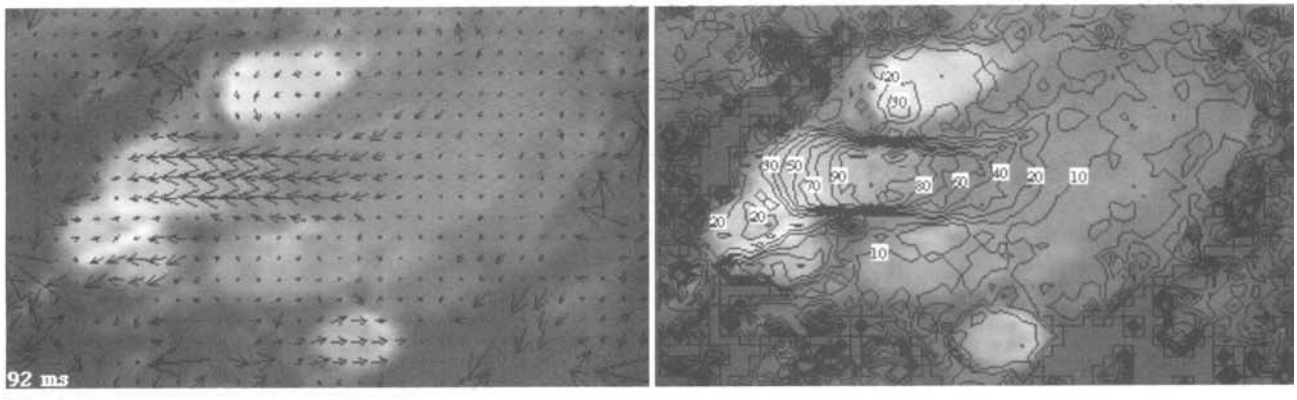

2b.

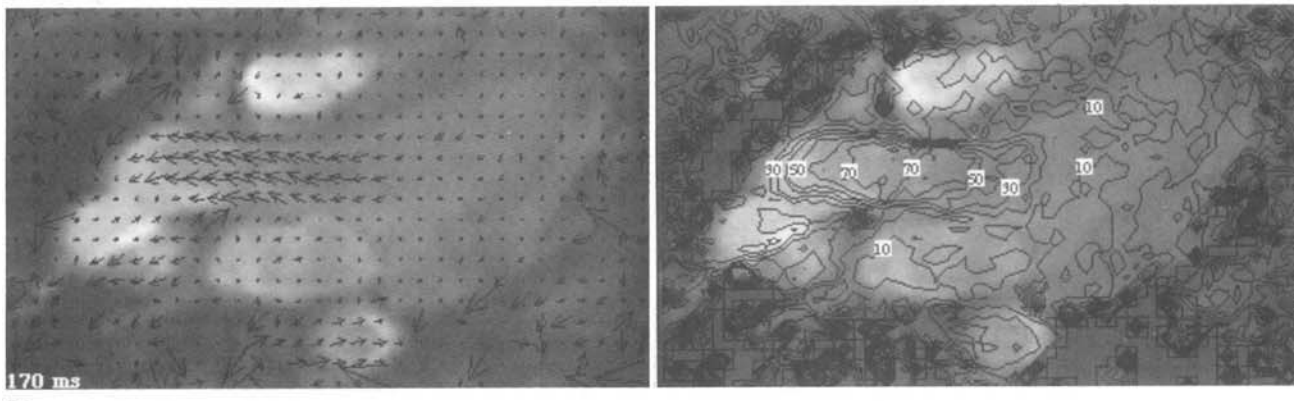

2c.

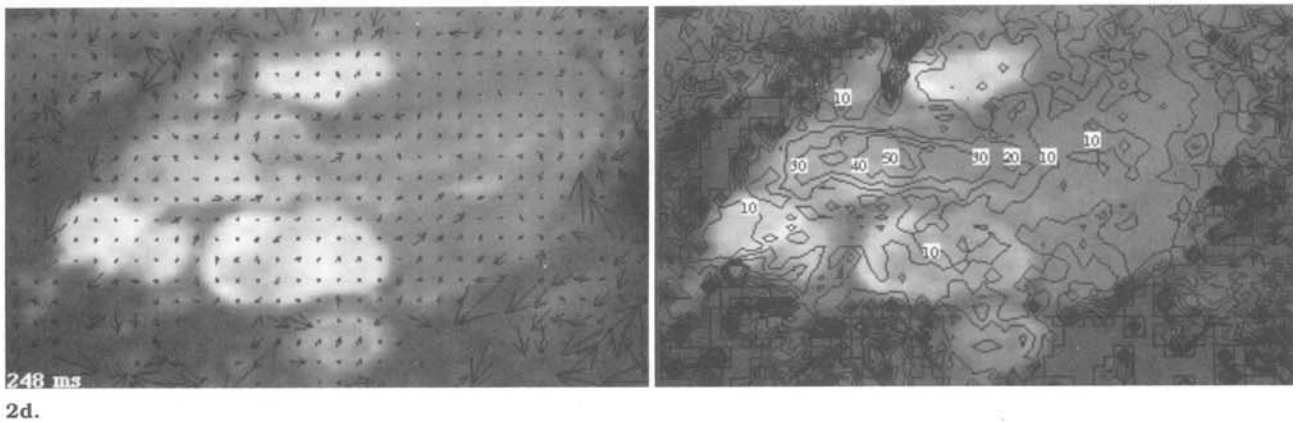

2d.

Figure 2. Vector plots (left) and corresponding contour plots (right) obtained at 14 **(a)**, 92 **(b)**, 170 **(c)**, and 248 **(d)**, msec after R wave (*Fig 2 continues*).

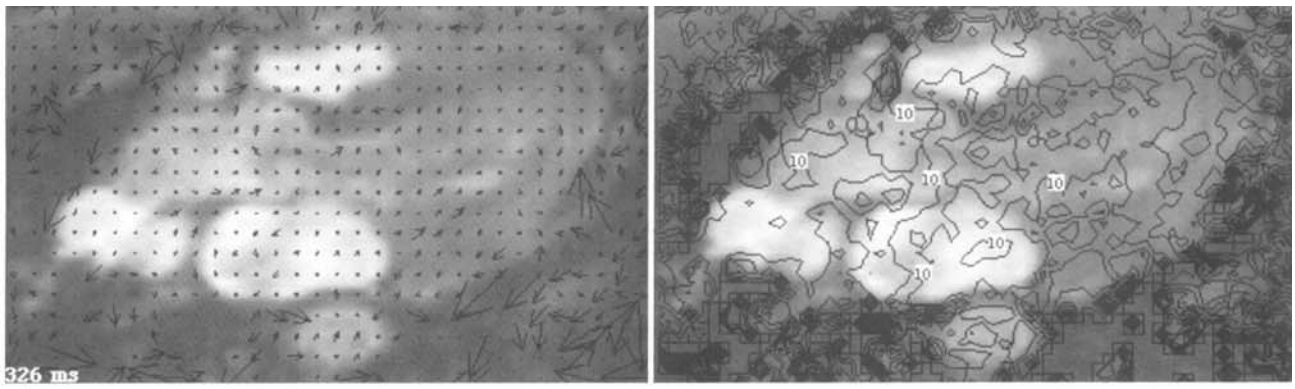

2e.

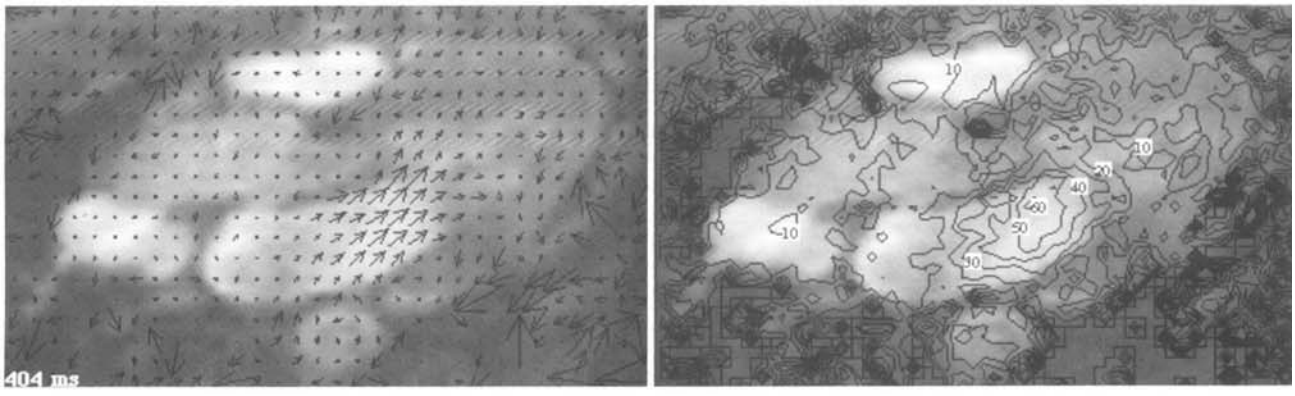

2f.

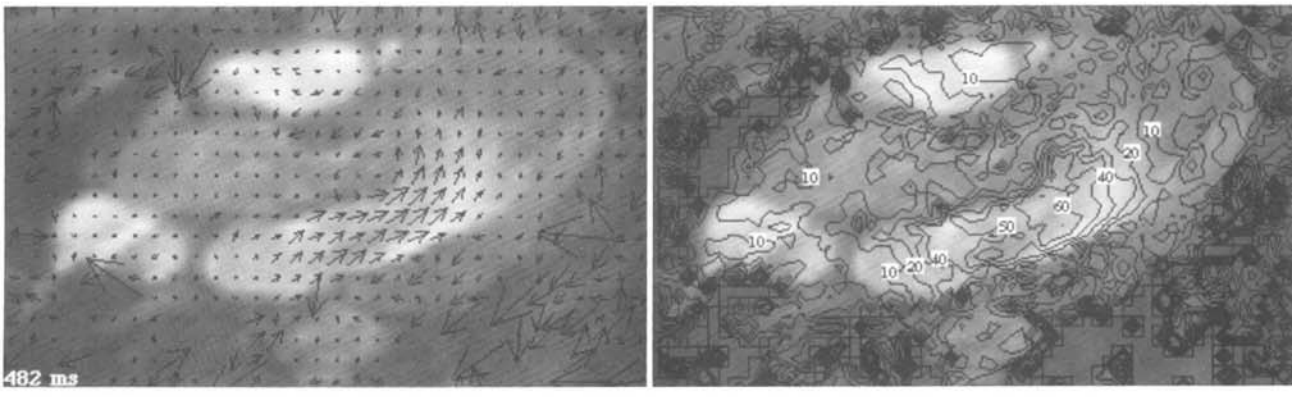

2g.

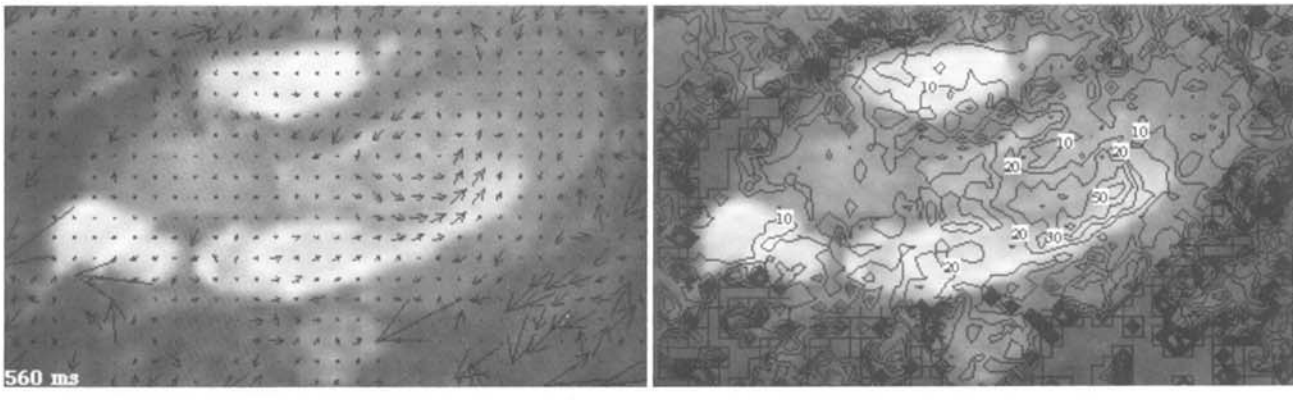

2h.

Figure 2 (*continued*). Vector plots (left) and corresponding contour plots (right) obtained at 326 **(e)**, 404 **(f)**, 482 **(g)**, and 560 **(h)** msec after R wave (*Fig 2 continues*).

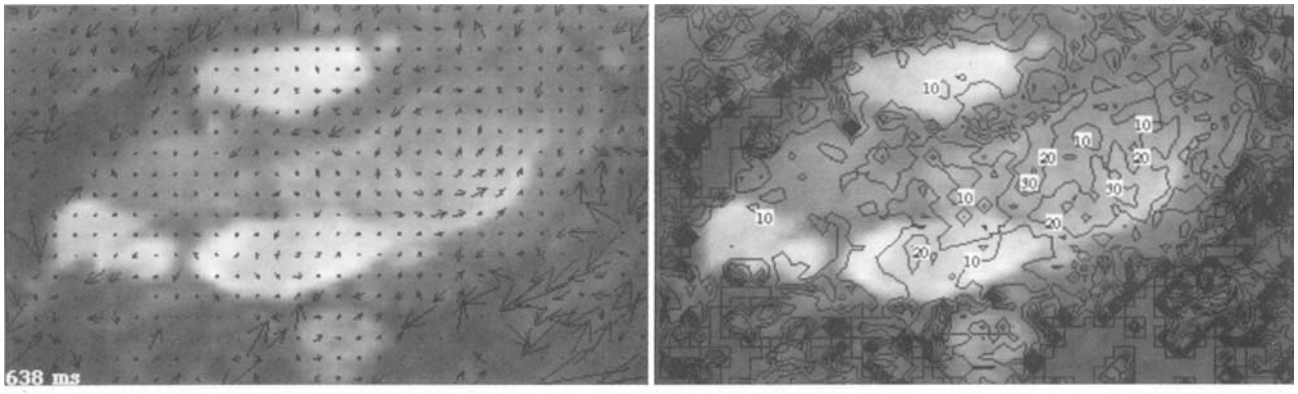

2i.

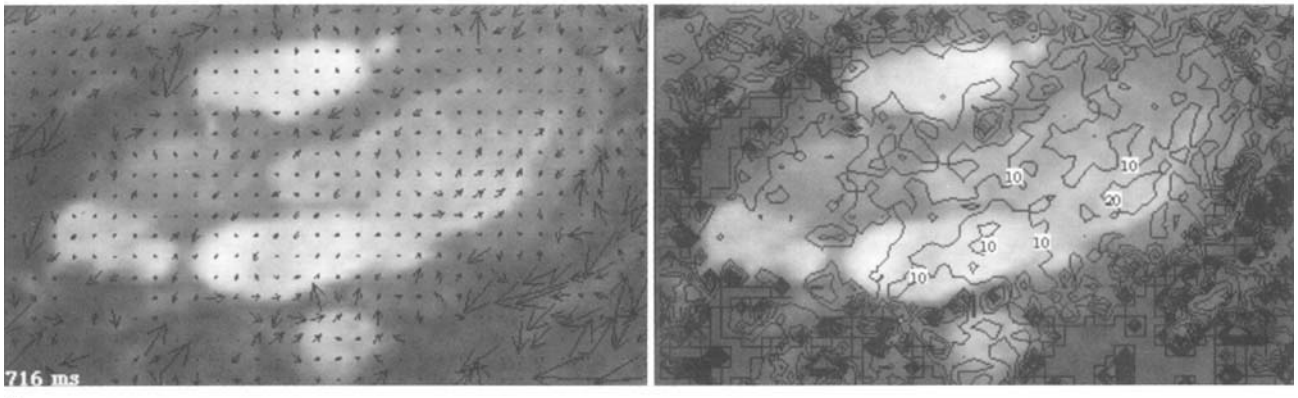

2j.

Figure 2 (*continued*). Vector plots (left) and corresponding contour plots (right) obtained at 638 **(i)** and 716 **(j)** msec after R wave. Numbers on contour plots indicate velocity in centimeters per second. *Ao* = aorta, *DEC Ao* = descending aorta, *LA* = left atrium, *LV* = left ventricle, *PA* = pulmonary artery, *RA* = right atrium, *SCV* = superior vena cava.

arrows is proportional to velocity, the contour plots provide a more readable means of displaying the velocity magnitude.

Figure 2a shows the start of systole, just after the opening of the aortic valve. The flow in the LVOT is visible, and the ventricle is distended, with little flow inside. The aortic velocity is about 30 cm/sec.

Figure 2b shows the flow close to peak ejection. Aortic flow has increased to about 1 m/sec and is skewed toward the anterior side of the aorta. The left ventricle is distended, with flow on the order of 10 cm/sec inside. Flow is visible in the descending aorta and is on the order of 40 cm/sec. Flow can also be seen in the right atrium at the top of the image and in the pulmonary artery on the left.

After peak systole, the flow in the aorta decelerates, as shown in Figure 2c and 2d. Finally, at about 326 msec after the R wave, the aortic valve has closed (Fig 2e). In Figure 2e, the aorta appears distended and there is evidence of rotary flow in the sinus of Valsalva. There is little flow in any of the heart chambers. The left atrium appears larger and the left ventricle smaller relative to earlier images, although as the chambers move through the imaging plane because of cardiac motion, the imaging section may cut the chamber at a location in which the cross section is smaller.

Figure 2f shows the flow 78 msec after that in Figure 2e, at the start of diastole. The mitral valve has opened, and the anterior leaflet can be seen as the dark horizontal line across the center of the image. Blood can be seen exiting the left atrium and flowing into the ventricle. The region of maximum flow velocity is near the anterior leaflet of the mitral valve, and the velocity is on the order of 60 cm/sec. There is little flow in the region of the aortic valve because it is sheltered by the anterior leaflet of the mitral valve.

Figure 2g and 2h show the flow later in diastole, 482 and 560 msec after the R wave. The flow through the mitral valve has a similar maximum as before but is constant across the full width of the mitral valve orifice. The mitral valve has closed a little, allowing blood to flow between the anterior mitral leaflets and the interventricular septum toward the aortic valve.

Figure 2i shows the flow 638 msec after the R wave, late in diastole, with the mitral valve closing. The motion of the valve creates a large counterclockwise eddy inside the left ventricle.

The last image (Fig 2j) shows the flow just after the mitral valve has closed, 716 msec after the R wave. The eddy inside the left ventricle is still present, and there is evidence that this eddy is present in Figure 2a, in which the aortic valve has just opened, although velocities as low as this are unreliable.

• DISCUSSION

Data Analysis

It is evident from Figure 1a that after subtraction of the flow-compensated phase image from the flow-encoded phase image, there remains a background phase error. For the data presented here, the background error is negative. This reduces the velocity values of the data and gives the initial velocity image (Fig 1a) a dark appearance. For purely visual assessment of velocity, an image of this type is adequate; however, for more quantitative use of the velocity field, this background error will substantially affect the accuracy of the data. It is necessary, therefore, to remove this error before quantitative use is made of the data.

The first step in this procedure is to calculate the standard deviation image. This image is a measure of the magnitude of the velocity fluctuations over a cardiac cycle in each voxel. Static regions, even if they have an offset in their magnitude, will have a low standard deviation because this offset does not vary greatly over the cardiac cycle.

It was found that these regions (Fig 1d) correspond to areas of both blood and tissue. Although most areas of blood are pulsatile, they can be included in the static regions if there is no major velocity component in the measured velocity direction. Other areas, which may include tissue, can conversely be excluded from the static regions if the tissue moves throughout the heart cycle. This motion can either be registered as a velocity or bring high-velocity blood regions into the voxel.

The accuracy with which the static regions can be located will depend on the threshold limit on the standard deviation. In the above analysis, this limit was set so that 15% of the data was defined as static. The static regions identified in this manner can be checked by viewing an animation of the modulus image with the static regions marked in red. This animation should show no conflict between the defined static regions and the moving fluid. If this is not so, the percentage of data defined as static can be changed. In our experience, the 15% value is usually good for cardiac applications. A less sensitive choice for the static tissue can be applied if a larger field of view is used. Using a full torso image reduces the influence of the static regions close to the heart and includes static muscle regions in other areas of the torso. These muscle regions are more reliable, because the heart regions are subject to cardiac motion.

One cause of inaccuracy in this method is the linear approximation to the background phase. If the background phase variation over the image is highly nonlinear, the correction to the velocity will be invalid in certain places. This can be corrected by the use of a higher-order surface fit to the background error. The accuracy of the removal of the background error can be assessed by studying the size of the velocity vectors on the images in Figure 2. In those regions surrounding the heart in which the velocity should be near zero, the vectors are seen to be small. This is found across the whole image, indicating that there is no substantial velocity offset or velocity gradient present. The direction of the vectors is consistent with the geometry of the heart, with no flow appearing to be directed through the heart walls. This is also evident on the contour plots, which follow the outlines of the left ventricle and aorta very closely. Note that in Figure 2d, there is no velocity in the thin region in which the open anterior mitral valve leaflet is found. As an indication of the accuracy of the background phase subtraction, a mean value was obtained from an 8 × 8-pixel square at the top left corner of the average image and from the background error (*BGE*) and final velocity images (*Vel Noise*) in Figure 1. This position was chosen because it is defined as a static region in Figure 1d and should therefore have a zero mean velocity after error subtraction. It was found that the mean of the average velocity in this region before error subtraction was −60.5 cm/sec, the mean of the background error was −60.0 cm/sec, and the mean of the final velocity was −1.9 cm/sec. These results show that (*a*) there is a substantial initial phase error over the image, (*b*) this error is close to being constant at this location, and (*c*) the above process can reduce this error—at least relative to the magnitude of the main blood velocities. No direct comparison between the MR-measured velocity and an independent source (such as Doppler ultrasound) was available for these data. Other authors have, however, measured complex flow fields by using MR phase velocity encoding and comparing the results to known values. They found good agreement between the MR velocity and the true velocity (13–16), except in regions with high turbulence or high spatial acceleration (13,14). High spatial acceleration is generally caused by a narrowing of the vessel cross section, such as that due to a stenosis. The acceleration produced by such a stenosis is not present in the normal left ventricle and cannot produce errors in Figure 2. For velocity measurements in diseased hearts—in particular those with aortic or mitral stenosis—the extreme decrease in cross-sectional area at the level of the valve will create considerable acceleration effects that will substantially affect the accuracy of velocity measurement. A reduction in TE will be needed to reduce these effects (17).

It has been reported that aortic MR angiograms obtained with the same gradient sequence produce the best information on disease if the image is obtained during peak systole (12). In grading these images, attention was paid to the contrast between moving blood and surrounding tissue. With this criterion, the best contrast occurs when blood is flowing fastest. This does not necessarily mean that the quality of the image signal is poor during other times in the cardiac cycle. In fact, it has been shown that for a typical systolic acceleration of 10 m/sec^2, the error in the phase is only 3 cm/sec (16). Temporal acceleration is unlikely, therefore, to introduce large errors.

Errors in the output may also result if the velocity exceeds the maximum velocity encoded, and aliases. In this case, the velocity vectors will be incorrect. As yet, no correction has been made for this, and it remains up to the user to correctly predict the maximum velocity in the region of interest, to prevent incorrect images.

Noise Reduction

Noise reduction must be performed on the images to prevent inordinately large velocity data from mar-

ring the vector and contour plots. Noise was found to create large variations in velocity measurements. The standard deviation image can therefore be used to locate noisy regions, because these regions will have a large standard deviation. The regions with the largest standard deviation are shown in white in Figure 1c. The relative brightness of these regions indicates that the noise has a large amplitude fluctuation relative to other regions of the image, such as those corresponding to the flow in the heart or in the static regions. This permits us to accurately locate the noisy regions and set their velocity equal to zero without affecting the velocity data in other regions. This can be seen in Figure 1g, which shows the regions of noise for this set of data. In this image, there are no false-positive regions; in other words, no regions within the heart have been identified as noise. As with the identification of the static regions, the effectiveness of this step can be checked by viewing the corrected images. If it is found that too much of the data has been lost or not enough noise has been removed, then the limit can be changed accordingly.

Figure 1h shows the result of setting the noise regions to zero. There are still some regions of noise, but most have been removed. In future studies, the modulus images will be used to aid in the identification of noisy regions, as these regions generally appear dark (18). This coupling of modulus image to phase is not always desirable, however, because it can lead to problems if there is a reduction in the signal level due to high-velocity flow, such as may appear in pathologic cases. Although the signal intensity is reduced in these images, the phase signal—and therefore the velocity—may still be preserved. Under such conditions, the deletion of velocity information on the basis of the modulus image will result in the loss of good data. This problem is prevented with the method presented here, since there is no coupling of modulus and phase images. Another method is to use a modulus-weighted phase image, which reduces the level of noise in regions of low signal intensity (19). This method is useful for angiographic images but not for quantitative vector or contour plots, since the velocity information is incorrect.

Visualization

After the above error corrections, the vector and contour plots seen in Figure 2 were generated. These images clearly show the flow of blood through the left side of the heart over the cardiac cycle. The images indicate a great deal about the nature of the flow in the left ventricle. They show the change in the flow of blood through the left side of the heart and the interaction of the blood with the heart walls and the aortic and mitral valves.

The simultaneous visualization of the two-dimensional blood flow across the whole LVOT allows a clear insight into the flow field. This insight is even more enhanced if the vector images are animated. We have done this with a Macintosh computer and found that the addition of motion to the vector plots reveals a great deal about the time-dependent nature of the flow.

This study was limited to flow in the left ventricle in one healthy volunteer, and conclusions drawn about the nature of the flow are confined to this particular heart, although it is hoped they are generally applicable. Further studies will therefore be necessary to confirm these results and to obtain a "normal" flow pattern for the healthy human heart. It will be interesting to apply this technique to cases of abnormal heart function to observe the effect of the abnormality on blood flow and, perhaps more important, to see what effect the blood flow has on heart and valve performance. The acceptable imaging time (15 minutes) makes this possible, and it is hoped that in the near future more clinically important cases will be presented. The analysis time is also short, requiring only 5 minutes on the Personal Iris workstation. This computer has comparable speed to that of the 486 PC and low-end Vax machines. A similar set of programs running on a Sun computer (Sun Microsystems, Mountain View, Calif) was, however, faster. The technique could, therefore, be applied in the clinical setting.

• CONCLUSIONS

This study has demonstrated the following:

1. An approximation to the background phase error can be found by fitting a plane surface to the static regions of the velocity images. These regions can be accurately identified from an image representing the time standard deviation of the velocity over a cardiac cycle. The static regions correspond to the low-standard-deviation areas of this image.

2. Regions of noise can also be identified from the standard deviation data. In this case, the noisy regions corresponded to the high-standard-deviation areas.

3. By presentation of the error-corrected velocity data in contour and vector form, projected on the normal MR modulus images, an excellent understanding of both the magnitude and direction of the blood flow field can be obtained over the cardiac cycle.

4. Because it is an automated procedure, this analysis can be installed in the clinical setting.

5. Further studies applying this technique to pathologic cases promise to bring further insight into the role of blood flow in cardiac disease. ●

References

1. Okano M, Yoshida Y. Endothelial cell morphology of atherosclerotic lesions and flow profiles at aortic bifurcations in cholesterol fed rabbits. J Biol Eng 1992; 114:309–316.
2. Caro CG, Fitz-Gerald JM, Schroter RC. Arterial wall shear and distribution of early atheroma in man. Nature 1969; 223:1159–1161.
3. Schettler G, Nerem RM, Schmid-Schonbein H, Diehm C, eds. Fluid dynamics as a localization factor for atherosclerosis. Berlin, Germany: Springer-Verlag, 1983; 110–145.
4. Yoshida Y, Wang S, Okano M, Oyama T, Yamane T, Mitsumata M. The effect of augmented hemodynamic forces on the progression and topography of atherosclerotic plaques. Ann NY Acad Sci 1990; 598:256–273.
5. Lefebvre X, Gieseking ER, Cape EG, Yoganathan AP. Steady flow visualization of the systolic anterior motion of the mitral valve in hypertrophic cardiomyopathy: an in vitro study. J Biomech Eng 1992; 114:406–413.
6. Delemarre BJ, Visser A, Bot H, Dunning AJ. Prediction of apical thrombus formation in acute myocardial infarction based on left ventricular spatial flow pattern. J Am Coll Cardiol 1990; 15:355–360.
7. Klipstein RH, Firmin DN, Underwood SR, Ree RSO, Long-

more DB. Blood flow patterns in the human aorta studied by magnetic resonance. Br Heart J 1987; 58:316–323.
8. Meier D, Maier S, Boesiger P. Quantitative flow measurements on phantoms and on blood vessels with MR. Magn Reson Med 1988; 8:25–34.
9. Mohiaddin RH, Wann SL, Underwood R, Firmin DN, Rees S, Longmore DB. Vena caval flow: assessment with cine MR velocity mapping. Radiology 1990; 177:537–541.
10. Moran P. A flow velocity zeugmatographic interlace for NMR imaging in humans. Magn Reson Imaging 1982; 1:197–203.
11. Dulce MC, Mostbeck GH, O'Sullivan M, Cheitlin M, Caputo GR, Higgins CB. Severity of aortic regurgitation: interstudy reproducibility of measurements with velocity-encoded cine MR imaging. Radiology 1992; 185:235–240.
12. Lanzer P, McKibbin G, Bohning D, et al. Aortic iliac imaging by projection phase sensitive MR angiography: effects of triggering and timing of data acquisition on image quality. Magn Reson Imaging 1990; 8:107–116.
13. Sun Y, Hearshen DO, Rankin GW, Haggar AM. Comparison of velocity-encoded MR imaging and fluid dynamic modeling of steady and disturbed flow. JMRI 1992; 2:443–452.
14. Ku DN, Oshinski JN, Markou CP, Pettigrew RI. Some errors in magnetic resonance flow measurements resulting from fluid dynamics (abstr). Biomech Symp 1991; 120:41.
15. Wehrli FW, Shimakawa A, MacFall JR. MR imaging of venous and arterial flow by a selective saturation-recovery spin echo (SSRSE) method. J Comput Assist Tomogr 1985; 9:537–545.
16. Duerk JL, Pattany PM. In-plane flow velocity quantification along the phase encoding axis in MRI. Magn Reson Imaging 1988; 6:321–333.
17. Kilner PJ, Firmin DN, Rees RSO, et al. Valve and great vessel stenosis: assessment with MR jet velocity mapping. Radiology 1991; 178:229–235.
18. Firmin DN, Nayler GL, Klipstein RH, Underwood SR, Rees RSO, Longmore DB. In vivo validation of MR velocity imaging. J Comput Assist Tomogr 1987; 11:751–756.
19. Pelc NJ, Bernstein MA, Shimakawa A, Glover G. Encoding strategies for three-direction phase-contrast MR imaging of flow. JMRI 1991; 1:405–413.